

Magnetic nanoparticles in a nematic channel: A one-dimensional study

Konark Bisht,^{1,*} Varsha Banerjee,^{1,†} Paul Milewski,^{2,‡} and Apala Majumdar^{2,§}

¹*Department of Physics, Indian Institute of Technology Delhi, New Delhi 110016, India*

²*Department of Mathematical Sciences, University of Bath, Bath BA2 7AY, United Kingdom*



(Received 9 March 2019; published 10 July 2019)

We study a dilute suspension of magnetic nanoparticles in a nematic-filled channel and how the spatial magnetization \mathbf{M} can be tailored by the nematic anisotropy. We study the spatial configurations as stable critical points of a generalized phenomenological energy for a dilute ferronematic in the absence of external magnetic fields. We show how spatial inhomogeneities in the equilibrium nematic profile, induced by confinement and boundary effects, generate nonzero spatially inhomogeneous magnetization profiles in the system. Depending on the magnetonematic coupling energy, \mathbf{M} can either follow the nematic profile for large coupling or exhibit distinct polydomain structures separated by defect lines for weak coupling and low temperatures. Some exact solutions for prototypical situations are also obtained.

DOI: [10.1103/PhysRevE.100.012703](https://doi.org/10.1103/PhysRevE.100.012703)

I. INTRODUCTION

Nematic liquid crystals (NLCs) have constituent asymmetric molecules, e.g., rodlike or disklike molecules; they are classical examples of anisotropic materials with long-range orientational ordering or “special” directions of averaged molecular alignment, referred to as directors in the literature [1]. These special directions make NLCs directional in nature, with a direction-dependent response to external fields; indeed the directional coupling to light and electric fields makes NLCs the working material of choice for the display industry. However, the NLC response to magnetic fields is relatively weak, e.g., fields larger than 1 kOe are needed to reorient nematic molecules [1–3]. In the 1970s, Brochard and de Gennes suggested that the addition of magnetic particles to a NLC matrix could substantially increase the magnetic response of the colloidal suspension and create a class of soft matter systems with a net nonzero magnetization even in the absence of external magnetic fields, referred to as ferronematics [3]. These were subsequently realized experimentally by Rault, Cladis, and Burger [4] but the suspensions were rather unstable. Recently, Mertelj *et al.* [5] experimentally demonstrated a stable dilute ferronematic system, without segregation or flocculation effects, and the stability is an intricate consequence of plateletlike shapes of the magnetic nanoparticles (MNPs), polydispersity, and, importantly, the mechanical coupling between the MNPs and the host medium.

There are typically two experimental methods for MNP-NLC suspensions, as discussed in the literature [5–7]. In the first case, the suspension is quenched from the (disordered) isotropic phase to the (ordered) nematic phase in the presence of an external magnetic field. There are prescribed boundary

conditions for the nematic molecules and these boundary conditions impose a uniform nematic alignment along a common spatially homogeneous direction, described by a director field \mathbf{n} . The nematic molecules have antipodal symmetry so that \mathbf{n} and $-\mathbf{n}$ are physically equivalent [1]. The external magnetic field is applied along \mathbf{n} and the strong coupling between the external field, the magnetic moments of the MNPs, the nematic molecules, and the homogeneous boundary conditions creates a single-domain structure with almost uniform magnetization (along \mathbf{n}). In the second method, the MNP-NLC suspension is not subjected to special boundary conditions and is quenched in the absence of an external magnetic field. Consequently, there is only short-range nematic and magnetic order. Although the magnetic moments are parallel to \mathbf{n} , they are equally likely to point along \mathbf{n} or $-\mathbf{n}$ directions. Consequently, the macroscopic magnetization vanishes and such a suspension is called a *compensated ferronematic* [6].

We study a model problem motivated by the experimental setup of platelet-shaped MNPs suspended in a NLC system, as in [5]. We study a dilute ferronematic suspension in a two-dimensional (2D) channel defined by

$$\Omega = \{(x, y) \in \mathbb{R}^2 : 0 \leq y \leq d; -D \leq x \leq D\} \quad (1)$$

such that $D \gg d$. We assume that the structural characteristics only vary in the y direction so that the system is invariant in the x direction. This is a reasonable assumption for a long, thin system with certain types of boundary conditions. The channel dimensions are assumed to be on the micron scale and the platelets have dimensions on the nanometer scale, as in [5]. In contrast to previous studies of ferronematics in confinement [8], we impose conflicting boundary conditions for the nematic molecules on the bounding surfaces, $y = 0$ and $y = d$, i.e., planar on one surface and homeotropic (or normal) on the other, so that the equilibrium nematic profile is inhomogeneous. In [8], for example, the authors impose planar boundary conditions for the nematic profile, on $y = 0$ and $y = d$, leading to a homogeneous equilibrium nematic profile. We denote the averaged spatial magnetization

*Konark.Bisht@physics.iitd.ac.in

†varsha@physics.iitd.ac.in

‡P.A.Milewski@bath.ac.uk

§a.majumdar@bath.ac.uk

vector by \mathbf{M} , induced by the magnetic moments of a dilute suspension of MNPs in a NLC. Additionally, we impose boundary conditions for the magnetization vector, \mathbf{M} , on the surfaces $y = 0$ and $y = d$; this could be achieved by applying an external field along the boundaries that aligns the MNPs on the boundaries in a certain direction and then fixing the MNPs in terms of position and orientation on these boundaries. We work with low temperatures that favor nematic ordering and nonzero magnetization in the bulk without any external effects. In particular, we have an inhomogeneous equilibrium nematic profile dictated by conflicting boundary conditions. Our system could be experimentally realized in different ways. One mechanism involves quenching the system from high temperatures to low temperatures, perhaps in the presence of a magnetic field and letting the system relax into equilibrium. The magnetic field biases the interior \mathbf{M} profile too, since \mathbf{M} tends to align with the external magnetic field. We then remove the magnetic field, with fixed boundary conditions for the nematic order and \mathbf{M} , and model the long-time equilibrium spatial profiles at a fixed low temperature, which are influenced by the energies associated with a spatial field \mathbf{M} , the nematic elasticity, and, crucially, the coupling between the NLC and MNPs.

We have two essential macroscopic variables in this problem—the nematic order parameter modeled by a Landau–de Gennes order parameter \mathbf{Q} , which contains information about both the directions and degree of nematic ordering, and the spatial magnetization, \mathbf{M} , which is induced by the coupling between the magnetic moments of the MNPs and the surrounding nematic molecules. The Landau–de Gennes \mathbf{Q} order parameter is a matrix, whose leading eigenvector, denoted by \mathbf{n} , models the locally preferred direction of nematic alignment. The magnetization, \mathbf{M} , is a 2D vector and, in particular, we allow \mathbf{M} to have variable magnitude, including $\mathbf{M} = \mathbf{0}$, to account for segregation effects as in [8]. For example, one might expect MNPs to migrate away from nematic defects or regions of large nematic distortion, and such regions have zero local magnetization. In fact, one could propose that nodal lines or zero lines of \mathbf{M} are the mathematical signature of the domain walls reported in [5,9], that separate polydomains of distinct magnetizations. We work with a generalized version of the phenomenological energy of a dilute ferronematic used in [5] and later rigorously justified from a microscopic model in [8]. The energy has three contributions—the Landau–de Gennes energy of a NLC [1], the Landau energy associated with a nonzero \mathbf{M} field with a stiffness term that penalizes spatial inhomogeneities in \mathbf{M} [10], and a magnetonematic coupling energy. We do not include the entropic term as in [11] since we follow the continuum approach developed in [5,8] with modifications, for a dilute suspension. The stable configurations are modeled as global or local minimizers of this phenomenological energy. As in previous work [5], we assume that \mathbf{M} preferentially locally aligns in the same direction as the nematic molecules, and this is the “soft anchoring” limit of the NLC-MNP coupling energy proposed in [11]. The coupling energy crucially depends on a coupling parameter, which in turn depends on the size, shape of the MNPs, the nematic elasticity, and, importantly, how strongly the NLC couples to a MNP and vice versa through MNP-surface mediated interactions [8,12].

Mathematically, we study Dirichlet boundary-value problems for \mathbf{Q} and \mathbf{M} that are derived from variational principles starting from a phenomenological energy as described above, with Dirichlet boundary conditions for both \mathbf{Q} and \mathbf{M} . There are three essential parameters in the problem—the nematic elasticity constant, the magnetic stiffness constant, and the magnetonematic coupling parameter. The governing partial differential equations have four key dimensionless parameters: $\{\ell_1, \ell_2, \xi, c\}$, incorporate the geometrical length scales, the intrinsic nematic correlation length, the magnetic coherence length, and the magnetonematic coupling strength. In what follows, we only study the equilibrium profiles in terms of the four dimensionless parameters and do not relate the observations to material-dependent and geometrical length scales. In the limit of small elasticity or strong coupling, the \mathbf{M} profiles are naturally tailored by the inhomogeneous \mathbf{Q} profiles, and there are no polydomains, but a smoothly inhomogeneous \mathbf{M} profile that describes the reorientation of the MNPs in response to the inhomogeneous \mathbf{Q} profile. In contrast, for strong nematic elasticity or weak magnetonematic coupling, the nematic and \mathbf{M} profiles are essentially decoupled. We numerically observe polydomains in both \mathbf{Q} and \mathbf{M} ; these polydomains are featured by a constant \mathbf{M} and a constant \mathbf{n} and are separated by domain walls with $\mathbf{Q} = \mathbf{0}$ and $\mathbf{M} = \mathbf{0}$. Both of these limits can be understood analytically using asymptotic methods. We numerically demonstrate the creation of these ordered polydomains by quenching the system and the loss of polydomain stability by increasing the magnetonematic coupling. Given that we are working at low temperatures, the numerically observed polydomains are not isotropic-nematic polydomains since the isotropic phase with $\mathbf{Q} = \mathbf{0}$ is unstable for low temperatures; in fact, they are ordered polydomains. Our numerical examples are not exhaustive, but they are interesting illustrations of how conflicting boundary conditions and geometric frustration can drive tailored morphologies and polydomain formation in ferronematics in the absence of external magnetic fields and such tailored morphologies open the door for bistable or multistable ferronematic systems in the near future, for new magnetomechanical effects in NLCs.

The paper is organized as follows. In Sec. II, we present the model and the governing equations. We numerically study the existence and stability of polydomains under model conditions in Sec. III. We present some conclusions and directions for future work in Sec. IV.

II. MODEL

In this section, we propose a variant of the phenomenological energy proposed in [5,8], based on the Landau–de Gennes (LdG) theory [1], whereas the approach in [5,8] follows the Oseen-Frank theory for NLCs.

Our domain has been defined in Eq. (1) to be a slab geometry, and we assume that all macroscopic variables only depend on y —the spatial variable along the width of the channel. In particular, we only consider two boundaries: $y = 0$ and $y = d$ as defined in Eq. (1). In the LdG framework, we model the NLC by a \mathbf{Q} -tensor order parameter which contains information about both the degree and directions of NLC orientational ordering, within its eigenvalues and eigenvectors,

respectively. In contrast, the Oseen-Frank approach models the state of a NLC by a unit-vector field, that represents the single preferred direction of local molecular alignment in space [1]. We work in a reduced 2D LdG framework for which the \mathbf{Q} -order parameter is a symmetric, traceless 2×2 matrix [13]; this reduced approach has been used with success for severely confined systems where the height of the system is much smaller than the cross-sectional dimensions (see for example [13]). The reduced LdG \mathbf{Q} -order parameter can be written as

$$\mathbf{Q} = s(2\mathbf{n} \otimes \mathbf{n} - I_2), \quad (2)$$

where \mathbf{n} is a 2D unit vector that models the distinguished direction of local nematic alignment in the plane, s is a scalar order parameter that measures the degree of order about \mathbf{n} , and I_2 is the 2×2 identity matrix. Mathematically, \mathbf{n} is an eigenvector of \mathbf{Q} with the largest eigenvalue (which is necessarily positive since \mathbf{Q} is traceless) and we can write $\mathbf{n} = (\cos \varphi, \sin \varphi)$ for some angle φ in the plane; care should be taken with this representation for topologically nontrivial boundary conditions but this is not problematic for our choice of boundary conditions. Further, \mathbf{Q} has two independent components, Q_{11} and Q_{12} , related to s and φ by

$$Q_{11} = s \cos 2\varphi, \quad Q_{12} = s \sin 2\varphi. \quad (3)$$

The isotropic phase corresponds to $\mathbf{Q} = 0$ or equivalently $s = 0$. In particular, if s is constant, then the state of the NLC is described by the eigenvector \mathbf{n} alone, and this reduces to the Oseen-Frank approach to modeling NLCs, as employed in [5,8]. The degree of orientational order is not accounted for in the Oseen-Frank approach, and the 2D LdG approach allows us to capture variations in the degree of order and potential domain walls or defects described by $s = 0$. In terms of boundary conditions, we impose homeotropic (or normal) conditions, given by $\varphi = \frac{\pi}{2}$ on $y = 0$, and planar conditions given by $\varphi = 0$ on $y = d$. In what follows, we use these conditions to prescribe suitable Dirichlet conditions for Q_{11} and Q_{12} .

The LdG theory is a variational theory; hence there is a LdG free energy density, f_{nem} , that drives pattern formation in NLCs [1,13]:

$$f_{\text{nem}}(\mathbf{Q}, \nabla \mathbf{Q}) = \frac{A}{2} |\mathbf{Q}|^2 + \frac{C}{4} |\mathbf{Q}|^4 + \frac{L}{2} \left(\frac{d\mathbf{Q}}{dy} \right)^2, \quad (4)$$

where $|\mathbf{Q}| = (\text{tr} \mathbf{Q}^2)^{\frac{1}{2}}$. The parameter $A = A_0(T - T_c^n)$ is effectively a rescaled temperature, where $A_0 > 0$ is a positive material-dependent constant and T_c^n is a characteristic nematic supercooling temperature related to the stability of the disordered isotropic phase. Loosely speaking, the isotropic phase is a stable critical point of $f_b(\mathbf{Q}) = \frac{A}{2} |\mathbf{Q}|^2 + \frac{C}{4} |\mathbf{Q}|^4$ for $A > 0$ and unstable for $A < 0$. We take $A < 0$ so that we work with low temperatures below the supercooling temperature which favor an ordered nematic texture with $s > 0$ in Eq. (2) and C, L are positive material dependent constants [13]. We note that the cubic term in the LdG bulk potential necessarily vanishes for 2D \mathbf{Q} tensors as in Eq. (2) but would appear for three-dimensional \mathbf{Q} tensors with five degrees of freedom. We employ a one-constant elastic energy density with a single

elastic constant L and further work includes the incorporation of elastic anisotropy.

The second contribution to the total energy of a dilute ferromagnetic is the energy density associated with a spatially varying magnetization field, \mathbf{M} , given by [10]

$$f_{\text{mag}}(\mathbf{M}, \nabla \mathbf{M}) = \frac{\alpha}{2} |\mathbf{M}|^2 + \frac{\beta}{4} |\mathbf{M}|^4 + \frac{\kappa}{2} \left(\frac{d\mathbf{M}}{dy} \right)^2. \quad (5)$$

This is the standard Landau energy, where α and β are Landau coefficients describing the ferromagnetic transition as in [5] and, additionally, we include an elastic energy density involving the stiffness constant $\kappa > 0$. By analogy with f_{nem} in Eq. (4), we take $\alpha < 0$ and $\beta > 0$ so that a nonzero \mathbf{M} is preferred for a spatially homogeneous system. On modeling grounds, we expect spatial inhomogeneities in \mathbf{M} to be energetically expensive in a system initially biased or quenched in the presence of an external magnetic field and this elastic term can also be justified on the grounds of nearest-neighbor interactions or by analogy with the kinetic energy term of quantum mechanical models [14,15]. This term prevents, for example, arbitrary rotations between \mathbf{M} and $-\mathbf{M}$ without an energetic cost in our phenomenological model. The third contribution is a magnetonematic coupling energy density, defined by analogy with the forms proposed in [5,11], with \mathbf{n} replaced by \mathbf{Q} as shown below:

$$f_c(\mathbf{Q}, \mathbf{M}) = -\frac{\gamma \mu_0}{2} M_i Q_{ij} M_j, \quad (6)$$

where Q_{ij} are the LdG order parameter components with $i, j = 1, 2$. The contribution of higher order magnetonematic coupling terms are not considered as the cubic coupling ($\sim \gamma$) is sufficient to induce magnetonematic ordering [16]. For s constant, this effectively reduces to $(\mathbf{n} \cdot \mathbf{M})^2$ as in [5]. The constant γ is a positive coupling constant that can be related to the shape and size of the MNPs and the strength of the surface-mediated MNP-NLC interactions via the surfaces of the MNPs. For our purposes, we do not focus on the microscopic details and simply interpret γ as a measure of the strength of the MNP-NLC coupling that coerces \mathbf{n} and \mathbf{M} to align with each other. The total energy density is the sum of f_{nem} , f_{mag} , and f_c as defined in Eq. (4), Eq. (5), and Eq. (6), respectively.

We employ the scaling $\mathbf{Q}' = \sqrt{2C/|A|} \mathbf{Q}$, $\mathbf{M}' = \sqrt{\beta/|\alpha|} \mathbf{M}$ for $\mathbf{M} = (\mathbf{M}_1, \mathbf{M}_2)$ and $y' = y/d$. The choice of the scaling factor necessarily means that $s = 1$ for the minimizers of the rescaled bulk potential $f_b(\mathbf{Q}')$ in Eq. (4), for $A < 0$. The rescaled energy density (dropping the primes) is (also see [13])

$$f(\mathbf{Q}, \mathbf{M}) := \frac{1}{4} \left[-|\mathbf{Q}|^2 + \frac{1}{4} |\mathbf{Q}|^4 + \ell_1 \left(\frac{d\mathbf{Q}}{dy} \right)^2 \right] + \frac{\xi}{2} \left[-|\mathbf{M}|^2 + \frac{1}{2} |\mathbf{M}|^4 + \ell_2 \left(\frac{d\mathbf{M}}{dy} \right)^2 \right] - \frac{c}{2} \{ Q_{11} (M_1^2 - M_2^2) + 2Q_{12} M_1 M_2 \}, \quad (7)$$

where

$$\ell_1 = \frac{L}{d^2|A|}, \quad \ell_2 = \frac{\kappa}{d^2|\alpha|}, \quad \xi = \frac{C}{|A|^2} \frac{|\alpha|^2}{\beta},$$

$$c = \frac{\gamma\mu_0}{|A|} \sqrt{\frac{C}{2|A|}} \frac{|\alpha|}{\beta}.$$

We model the stable configurations, (\mathbf{Q}, \mathbf{M}) , as local or global minimizers of the total energy

$$F[\mathbf{Q}, \mathbf{M}] := \int_0^1 f(Q_{11}, Q_{12}, M_1, M_2) dy, \quad (8)$$

since the rescaled boundaries are at $y = 0, 1$ and these minimizers are necessarily solutions of the corresponding Euler-Lagrange equations given below. Letting $\tilde{Q} = (|\mathbf{Q}|^2/2) - 1$ and $\tilde{M} = |\mathbf{M}|^2 - 1$, the equations are given by

$$\ell_1 \frac{d^2 Q_{11}}{dy^2} = \tilde{Q} Q_{11} - \frac{c}{2} (M_1^2 - M_2^2),$$

$$\ell_1 \frac{d^2 Q_{12}}{dy^2} = \tilde{Q} Q_{12} - c M_1 M_2,$$

$$\xi \ell_2 \frac{d^2 M_1}{dy^2} = \xi \tilde{M} M_1 - c (Q_{11} M_1 + Q_{12} M_2),$$

$$\xi \ell_2 \frac{d^2 M_2}{dy^2} = \xi \tilde{M} M_2 - c (Q_{12} M_1 - Q_{11} M_2). \quad (9)$$

In what follows, we interpret ℓ_1 as the nematic elasticity constant, ℓ_2 as the magnetic stiffness constant, ξ as a measure of magnetic order [large values of ξ coerce the system to minimize the magnetic energy f_{mag} in (5)], and c as a magnetonematic coupling constant. We point out that ℓ_1 is related to the ratio of the nematic correlation length to the geometric length scale d ; similarly, ℓ_2 is related to the ratio of the magnetic order parameter length to d . Since this manuscript is largely a proof of concept study of pattern formation in ferronematic systems without magnetic fields, we do not focus much on the numerical values of these parameters but rather on a qualitative study of the numerical solutions of (9) as a function of these parameters.

As a side remark, we can make the transformation $Q_{11} = |\mathbf{Q}| \cos \varphi / \sqrt{2}$, $Q_{12} = |\mathbf{Q}| \sin \varphi / \sqrt{2}$, $M_1 = M \cos \psi$, and $M_2 = M \sin \psi$ in Eq. (9), and check that we have an explicit branch of solutions of Eq. (9) given by

$$\varphi = \psi = ay + b, \quad |\mathbf{Q}| = Q^*, \quad |\mathbf{M}| = M^* \text{const} \quad (10)$$

for the Dirichlet conditions, $|\mathbf{Q}(0)| = |\mathbf{Q}(1)| = Q^*$, $M(0) = M(1) = M^*$, and $\phi = \psi$ at $y = 0, 1$. The constants a and b are set by the boundary conditions. The constant Q^* is determined as the positive real root of the cubic polynomial

$$Q^{*3} - pQ^* - \sqrt{2}q = 0 \quad (11)$$

and is given by

$$Q^* = \frac{2^{1/6} p}{3^{1/3} \Delta} + \frac{\Delta}{2^{1/6} 3^{2/3}} \quad (12)$$

provided $27q^2 > 2p^3$, where $p = 2 + c^2 - 8\ell_1 a^2$, $q = c\xi(1 - \ell_2 a^2)$, and $\Delta = (9q + \sqrt{3(27q^2 - 2p^3)})^{1/3}$. Finally, M^*

can be obtained from the relation

$$M^* = \sqrt{\frac{cQ^*}{\sqrt{2}} + \frac{q}{c}}. \quad (13)$$

III. NUMERICAL RESULTS

We prescribe Dirichlet conditions for \mathbf{Q} and \mathbf{M} and we impose perfect nematic ordering modeled by $s = 1$ on $y = 0$ and $y = 1$, with $\varphi = \frac{\pi}{2}$ on $y = 0$ and $\varphi = 0$ on $y = 1$. Mathematically, this translates to $Q_{11} = -1$ on $y = 0$ and $Q_{11} = 1$ on $y = 1$ [see Eq. (3)] with $Q_{12} = 0$ on both boundaries. We impose conflicting Dirichlet boundary conditions for \mathbf{M} , namely $\mathbf{M} = (-1, 0)$ on $y = 0$ and $\mathbf{M} = (1, 0)$ on $y = 1$. Given these conflicting boundary conditions, we cannot have uniform \mathbf{Q} or \mathbf{M} profiles, making this an interesting example of pattern formation in coupled systems.

We always have a branch of solutions with $Q_{12} = M_2 = 0$ for $0 \leq y \leq 1$ for this boundary-value problem; see Eq. (9) for all values of ℓ_1, ℓ_2, ξ, c . These solutions have a special physical interpretation—they describe polydomains. This can be simply understood since $Q_{12} = 0$ necessarily implies that $\varphi = 0$ or $\varphi = \frac{\pi}{2}$ everywhere in the interior (modulo a multiple of π), i.e., φ is a constant everywhere and jumps between the two distinct boundary values so that there are two distinct domains separated by a domain wall. These polydomains have finite energy since the domain wall is mathematically described by $\mathbf{Q} = \mathbf{0}$. Similar remarks apply to \mathbf{M} , since $|\mathbf{M}|$ is variable. If $M_2 = 0$ is identically zero everywhere, then M_1 smoothly mediates between the boundary values, $M_1 = -1$ (on $y = 0$) and $M_1 = 1$ (on $y = 1$), and there is again a domain wall with $\mathbf{M} = \mathbf{0}$ that separates two domains with $M_1 > 0$ and $M_1 < 0$, respectively. These polydomain structures are interesting but there is a necessary mismatch between the nematic alignment, modeled by $\mathbf{n} = (\cos \varphi, \sin \varphi)$ [in Eq. (2)] and $\mathbf{m} = \frac{\mathbf{M}}{|\mathbf{M}|}$ in regions where $\varphi = \frac{\pi}{2}$. It is reasonable to conjecture that these polydomain structures are energetically unfavorable for large c or small ℓ_1, ℓ_2 in Eq. (9) which effectively enforce stronger coupling between \mathbf{n} and \mathbf{M} . This can be made more precise in the language of asymptotic limits as discussed below.

Looking at the energy Eq. (8) and the system Eq. (9), we can see that very small values of ℓ_1, ℓ_2 coerce $\frac{|\mathbf{Q}|^2}{2} = Q_{11}^2 + Q_{12}^2$ and $|\mathbf{M}|^2 = M_1^2 + M_2^2$ to be unity almost everywhere [for minimizers of Eq. (8)], since this minimizes the gradient-free contributions or the bulk contributions to f_{nem} and f_{mag} in Eq. (7). We refer to this as the *Ginzburg-Landau limit* because of the close analogies with Ginzburg-Landau theory in this limit (see [17] for more details); the exact details are not relevant for this discussion. For simplicity, let us set $\ell_1 = \ell_2 = \ell$, $\xi = 1$, and c ; the key point is that, for ℓ small and for moderate to large values of $\frac{c}{\ell}$, we expect minimizers (\mathbf{Q}, \mathbf{M}) of Eq. (8) to have unit norm almost everywhere. This excludes polydomains with interior nodal lines defined by $\mathbf{Q} = \mathbf{0}$ and $\mathbf{M} = \mathbf{0}$, respectively. The relative magnitude of $\frac{c}{\ell}$ ensures that \mathbf{n} and \mathbf{M} tend to follow each other so that the two morphologies can be tailored by each other to yield smoothly inhomogeneous configurations. In contrast, the limit of large $\ell_1, \ell_2 \gg c$ is referred to as the *Laplace limit*, since the leading order equations in Eq. (9) are effectively just the Laplace equation for \mathbf{Q} and \mathbf{M} in this limit. From purely

heuristic arguments, one can deduce that energy minimizers will minimize the elastic energy in Eq. (8) to leading order, since the energetic penalty associated with variations in $|\mathbf{Q}|$ and $|\mathbf{M}|$ is small. Further, if the ratios $\frac{c}{\ell_1}, \frac{c}{\ell_2}$ are small, the cost of deviations between \mathbf{n} and \mathbf{M} are small. It is readily checked that the solution of

$$\frac{d^2 Q_{11}}{dy^2} = \frac{d^2 Q_{12}}{dy^2} = 0,$$

subject to boundary conditions $Q_{11} = -1$ on $y = 0$ and $Q_{11} = 1$ on $y = 1$, $Q_{12} = 0$ on both $y = 0$ and $y = 1$, is given by $Q_{11}(y) = 2y - 1$ and $Q_{12} = 0$ everywhere, with a domain wall at $y = \frac{1}{2}$. Crucially, linear profiles for Q_{11} and Q_{12} are the signatures of the Laplace limit and, because of the imposed boundary conditions, this naturally creates a domain wall with $\mathbf{Q} = \mathbf{0}$ in the interior. Analogous remarks apply to \mathbf{M} in the Laplace limit.

We only discuss a few selected scenarios for the four key parameters in this problem. There are other possibilities but our main aim is to give examples of model parameters which naturally allow polydomain formation and sets of model parameters which exclude polydomain formation, as illustrated by the numerical examples below. There are no rigorous results for the uniqueness of solutions of the system Eq. (9), but our numerical methods require an initial guess since they are based on the Newton algorithm. We have attempted several different initial guesses and they converge to the numerical solutions reported in this paper, on which grounds we deduce that the numerically computed solutions are at least local minimizers of the energy Eq. (8) under the prescribed conditions.

In Figs. 1(a) and 1(b), we plot a simple example of numerical solutions, \mathbf{Q} and \mathbf{M} , of the equations (9) with small values of ℓ_1, ℓ_2 , fixed $\xi = 1$, and $\frac{c}{\ell_1} = \frac{c}{\ell_2} = \frac{1}{100}$, i.e., weak elasticity and weak coupling. We observe that $|\mathbf{Q}|$ and $|\mathbf{M}|$ are both bounded away from zero; in fact, they are reasonably uniform in the interior and there are no polydomains, as predicted by the Ginzburg-Landau limit. The coupling c is relatively weak and the \mathbf{M} profile smoothly rotates between the prescribed boundary conditions. In Figs. 1(c) and 1(d) we illustrate the Laplace limit with $\ell_1 = \ell_2 = 10$ and strong coupling $c = 10$. There are distinct polydomains in the \mathbf{n} and \mathbf{M} profiles and it is interesting that the strong coupling does not induce any reorientation of $\mathbf{m} = \frac{\mathbf{M}}{|\mathbf{M}|}$ in the polydomain with $\varphi = \frac{\pi}{2}$ at the bottom [see Eq. (6)].

We further illustrate these concepts in Fig. 2, where we plot the solutions for \mathbf{Q} and \mathbf{M} with $\ell_1 = \ell_2 = 0.1$, $\xi = 1$ (with $Q_{11} = -1, M_1 = -1$ at $y = 0, Q_{11} = 1, M_1 = 1$ at $y = 1$, and $Q_{12} = M_2 = 0$ at $y = 0$ and $y = 1$). The elastic constants are intermediate and hence we are neither in the Ginzburg-Landau or Laplace limit. However, it is interesting that we get solutions with $Q_{12} = M_2 = 0$ everywhere for $c \leq 1$ and these solutions generate polydomains in \mathbf{n} and $\mathbf{m} = \frac{\mathbf{M}}{|\mathbf{M}|}$. The solution profiles for Q_{11} and M_1 are not perfectly linear as in Figs. 1(c) and 1(d) since we are away from the Laplace limit and hence Figs. 2(a)–2(d) are interesting examples of polydomain formation with moderate elasticity and relatively weak coupling. In Figs. 2(e) and 2(f), we can see clear signatures of strong coupling with very rapid reorientation

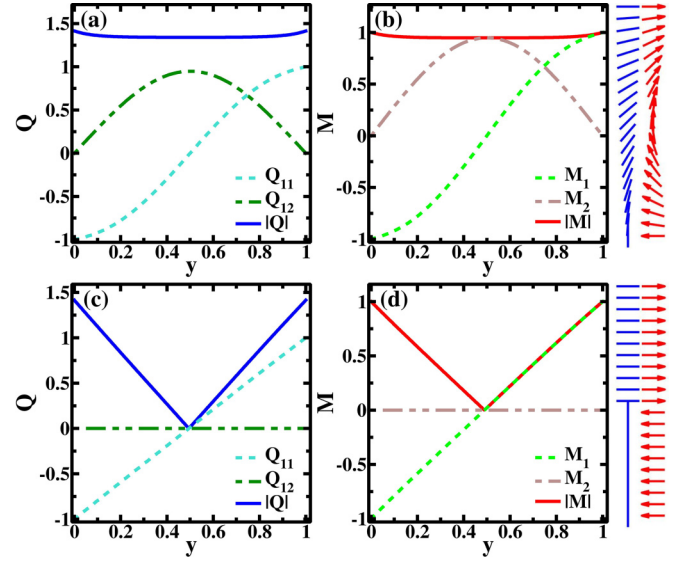


FIG. 1. Solutions of Eq. (9) under boundary conditions: $Q_{11}(0) = -1, Q_{11}(1) = 1, Q_{12}(0) = Q_{12}(1) = 0, \mathbf{M}(0) = (-1, 0)$, and $\mathbf{M}(1) = (1, 0)$ for Ginzburg-Landau limit ($\ell_1 = \ell_2 = 0.01, \xi = 1$, and $c = 0.0001$) in (a), (b) and for Laplace limit ($\ell_1 = \ell_2 = 10, \xi = 1$, and $c = 10$) in (c), (d). The vector plots show variation in \mathbf{n} (rods) and $\mathbf{m} = \frac{\mathbf{M}}{|\mathbf{M}|}$ (arrows) along the y axis.

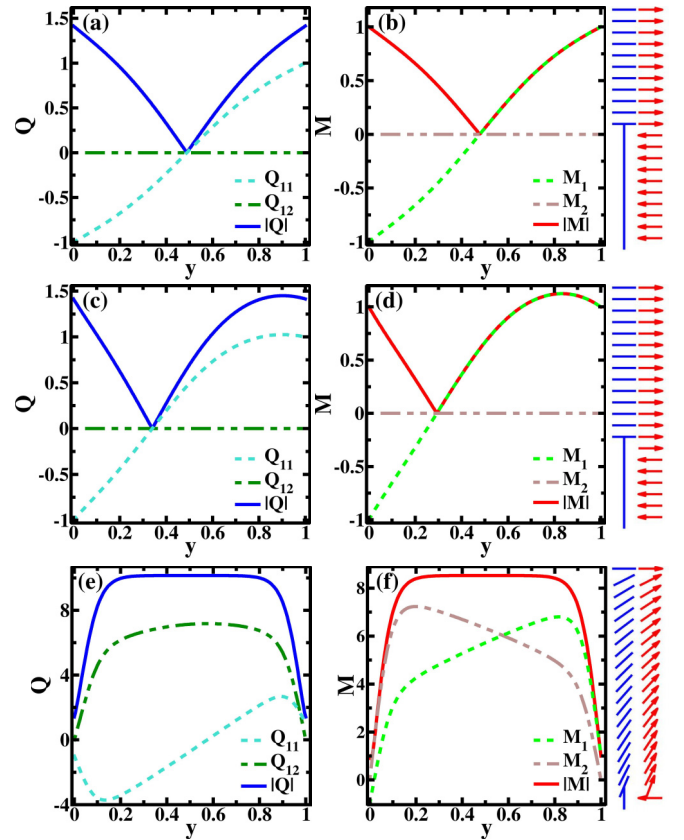


FIG. 2. Solutions of Eq. (9) under boundary conditions: $Q_{11}(0) = -1, Q_{11}(1) = 1, Q_{12}(0) = Q_{12}(1) = 0, \mathbf{M}(0) = (-1, 0)$, and $\mathbf{M}(1) = (1, 0)$. The plots (a), (b) are for $c = 0.1$, (c), (d) for $c = 1$, and (e), (f) for $c = 10$ with $\ell_1 = \ell_2 = 0.1$ for all the plots. We plot the unit-vector field \mathbf{n} as rods and the unit-vector field $\mathbf{m} = \frac{\mathbf{M}}{|\mathbf{M}|}$ as arrows.

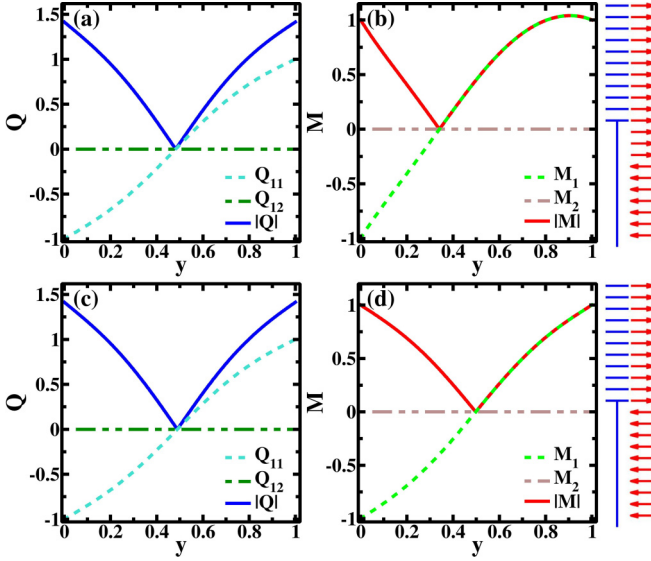


FIG. 3. Solutions of Eq. (9) under boundary conditions: $Q_{11}(0) = -1$, $Q_{11}(1) = 1$, $Q_{12}(0) = Q_{12}(1) = 0$, $\mathbf{M}(0) = (-1, 0)$, and $\mathbf{M}(1) = (1, 0)$. The solutions are obtained for $\ell_1 = \ell_2 = 0.1$, $c = 0.1$, and different values of ξ with $\xi = 0.1$ in (a), (b) and $\xi = 10$ in (c), (d). We plot the unit-vector field \mathbf{n} as rods and the unit-vector field $\mathbf{m} = \frac{\mathbf{M}}{|\mathbf{M}|}$ as arrows.

of \mathbf{M} in response to the reorientation of \mathbf{n} as defined in Eq. (2). However, the norm of $|\mathbf{Q}|$ or $|\mathbf{M}|$ does not tend to the Ginzburg-Landau value, owing to the relatively large values of the elastic constants.

In Fig. 3, we use the same values of ℓ_1 and ℓ_2 with $\xi \neq 1$ and $c \leq 1$. We get polydomains again with $Q_{12} = M_2 = 0$ everywhere. These polydomains are defined by points $y_Q \in (0, 1)$ for which $\mathbf{Q} = \mathbf{0}$ and $y_M \in (0, 1)$ for which $\mathbf{M} = \mathbf{0}$, respectively. At $y_Q \in (0, 1)$, we have $Q_{11}(y_Q) = Q_{12}(y_Q) = 0$ so that φ is not defined at y_Q and there is a jump discontinuity in \mathbf{n} at y_Q regularized by $|\mathbf{Q}| = \mathbf{0}$. This jump discontinuity is an example of a domain wall that separates two distinct regions with $\varphi = \frac{\pi}{2}$ on one side of the discontinuity and $\varphi = 0$ on the other side of the discontinuity. In general, $y_Q \neq y_M$ so that the two domain walls may not coincide. It is worth emphasizing that although $\mathbf{m} = \frac{\mathbf{M}}{|\mathbf{M}|}$ might be defined at $y_Q = 0$, $|\mathbf{M}(y_Q)|$ is small so that the degree of magnetization is small and we do not expect a concentration of MNPs near y_Q in the domain. Whilst the norm of the magnetization vector is small at the point y_Q , it need not be exactly zero so that some nonzero magnetization is retained. We do not analyze this further except to comment that the polydomain structure is preserved with $\xi \neq 1$ too, provided the coupling constant is not too large.

Next, we discuss the stability of the polydomain solutions or the solution branch with $Q_{12} = M_2 = 0$ everywhere, as a function of the coupling parameter c , for the boundary-value problem in Fig. 2. It is clear that we have a solution branch with $Q_{12} = M_2 = 0$ for all values of ℓ_1, ℓ_2, ξ, c . The numerics suggest that this solution branch loses stability for large c , since COMSOL [18] does not converge to solutions with polydomains for large c . We can provide some heuristics to

this effect. The coupling energy is

$$-\gamma\mu_0 M_i Q_{ij} M_j = \gamma\mu_0 s |\mathbf{M}|^2 \left(\frac{1}{2} - \cos^2 \theta_{\mathbf{nM}} \right),$$

where $\theta_{\mathbf{nM}}$ is the angle between the nematic director \mathbf{n} and the magnetization vector \mathbf{M} [also see Eqs. (2) and (3)]. The coupling energy is clearly minimized if \mathbf{n} and \mathbf{M} are perfectly aligned with each other. For solutions with $Q_{12} = M_2 = 0$, we have domain walls separating regions with $\varphi = \frac{\pi}{2}$, $\mathbf{m} = \frac{\mathbf{M}}{|\mathbf{M}|} = (-1, 0)$ from regions with $\varphi = 0$, $\mathbf{m} = \frac{\mathbf{M}}{|\mathbf{M}|} = (1, 0)$ and \mathbf{n} and \mathbf{m} are not aligned when $\varphi = \frac{\pi}{2}$ and $\mathbf{m} = (-1, 0)$. As c becomes larger, the energetic penalty for the mismatch between \mathbf{n} and \mathbf{M} increases and hence we get solutions as in Figs. 2(e) and 2(f) for which \mathbf{n} and \mathbf{M} align with each other, to minimize the dominant coupling energy. We also observe that $|\mathbf{Q}|$ and $|\mathbf{M}|$ tend to constants in the middle of the cell and this constant is greater than the boundary values of $|\mathbf{Q}|$ and $|\mathbf{M}|$. Referring to [19], the maximum principle dictates that the maximum value of $|\mathbf{Q}|$ and $|\mathbf{M}|$ (for uncoupled systems) is attained on the boundaries. In the Ginzburg-Landau and Laplace limits of these coupled systems, the system is maximally ordered at the boundaries but, for strongly coupled systems as in Figs. 2(e) and 2(f) the ordering seems to steadily increase in the bulk. This warrants further investigation and interpretation in the future. We illustrate this more conclusively by using the gradient flow model for the free energy in Eq. (8); the gradient flow model is based on the principle that systems evolve to a state of minimum energy or at least to a local energy minimizer according to the choice of initial conditions [20,21]. The governing partial differential equations are

$$\begin{aligned} \mu \frac{\partial Q_{11}}{\partial t} &= \ell_1 \frac{d^2 Q_{11}}{dy^2} - \tilde{Q} Q_{11} + \frac{c}{2} (M_1^2 - M_2^2), \\ \mu \frac{\partial Q_{12}}{\partial t} &= \ell_1 \frac{d^2 Q_{12}}{dy^2} - \tilde{Q} Q_{12} + c M_1 M_2, \\ \mu \frac{\partial M_1}{\partial t} &= \xi \ell_2 \frac{d^2 M_1}{dy^2} - \xi \tilde{M} M_1 + c (Q_{11} M_1 + Q_{12} M_2), \\ \mu \frac{\partial M_2}{\partial t} &= \xi \ell_2 \frac{d^2 M_2}{dy^2} - \xi \tilde{M} M_2 + c (Q_{12} M_1 - Q_{11} M_2), \end{aligned} \quad (14)$$

where $\mu > 0$ is a positive constant. We take $\ell_1 = \ell_2 = 0.1$, $c = 10$, $\xi = 1$, and $\mu = 5$. This is an initial boundary-value problem; the boundary conditions are as in Fig. 2. We need to prescribe initial conditions too. For initial conditions with $Q_{12} = M_2 = 0$, the solutions of the system Eq. (14) have $Q_{12} = M_2 = 0$ for all times. For slightly perturbed initial conditions, for example, with $Q_{12}(y, t = 0) = 0.01y(1 - y)$ and $M_2(y, t = 0) = 0.01y(1 - y)$, the solutions distinctly converge to solutions with nonzero Q_{12} and M_2 for long time, as illustrated in Fig. 4. This provides numerical illustration that the polydomain solutions are unstable critical points of the energy Eq. (8) in this parameter regime and hence COMSOL does not converge to these solutions in Fig. 2.

Finally, we look at the effects of temperature on polydomain formation in such systems. In [5], experiments show that fast quenching the sample from an isotropic state can produce a polydomain sample with two opposing states of magnetization. We try to numerically reproduce the same

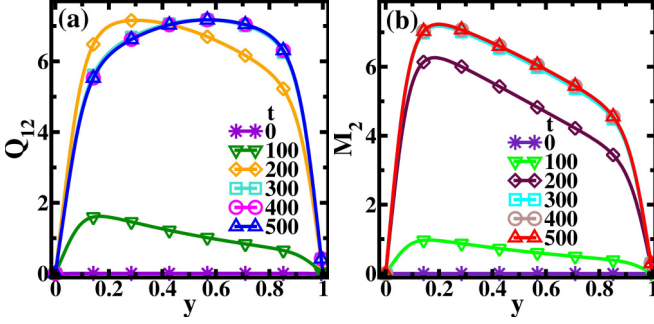


FIG. 4. Stability analysis for polydomain solutions with $Q_{12} = M_2 = 0$ everywhere [in Figs. 2(e) and 2(f)] by using gradient-flow method defined by Eq. (14) for parameters $\ell_1 = \ell_2 = 0.1$, $\xi = 1$, $c = 10$, and $\mu = 5$. The small perturbation $Q_{12}(y, t=0) = M_2(y, 0) = 0.01y(1-y)$ grows and converges to solutions with nonzero (a) Q_{12} and (b) M_2 for long time ($t \sim 500$). Markers are used to distinguish curves.

effect with a temperature parameter in the gradient-flow model in Eq. (14). The temperature dependent parameters are the Landau coefficients A and α in free energies f_{nem} and f_{mag} , respectively [Eqs. (4) and (5)]. At temperature T , we have $A = A_0(T - T_c^n)$ and $\alpha = \alpha_0(T - T_c^m)$, for critical temperatures T_c^n and T_c^m , respectively. For typical materials used in experiments, $T_c^m > T_c^n$ [22–25]. Let \bar{A} and $\bar{\alpha}$ be two characteristic fixed values of A and α , respectively; we then write the gradient-flow model as

$$\begin{aligned} \mu \frac{\partial Q_{11}}{\partial t} &= \ell'_1 \frac{d^2 Q_{11}}{dy^2} - \tilde{Q}_A Q_{11} + \frac{c'}{2} (M_1^2 - M_2^2), \\ \mu \frac{\partial Q_{12}}{\partial t} &= \ell'_1 \frac{d^2 Q_{12}}{dy^2} - \tilde{Q}_A Q_{12} + c' M_1 M_2, \\ \mu \frac{\partial M_1}{\partial t} &= \xi' \ell'_2 \frac{d^2 M_1}{dy^2} - \xi' \tilde{M}_\alpha M_1 + c' (Q_{11} M_1 + Q_{12} M_2), \\ \mu \frac{\partial M_2}{\partial t} &= \xi' \ell'_2 \frac{d^2 M_2}{dy^2} - \xi' \tilde{M}_\alpha M_2 + c' (Q_{12} M_1 - Q_{11} M_2), \end{aligned} \quad (15)$$

where $\tilde{Q}_A = \bar{A} + (|\mathbf{Q}|^2/2)$, $\tilde{M}_\alpha = \bar{\alpha} + |\mathbf{M}|^2$, and \bar{A} , $\bar{\alpha}$ are measures of the temperature. The rescaled parameters are defined by

$$\begin{aligned} \ell'_1 &= \frac{L}{d^2 \bar{A}}, \quad \ell'_2 = \frac{\kappa}{d^2 \bar{\alpha}}, \quad \xi' = \frac{C}{\bar{A}^2} \frac{\hat{\alpha}^2}{\beta}, \\ c' &= \frac{\gamma \mu_0}{\bar{A}} \sqrt{\frac{C}{2\bar{A}}} \frac{\hat{\alpha}}{\beta}. \end{aligned}$$

In the experiments, the system is initially at a high temperature $T_i > \max\{T_c^m, T_c^n\}$ (disordered phase) and then suddenly quenched to $T_f < \min\{T_c^m, T_c^n\}$ (ordered phase). The quenching, or sudden drop of temperature to $T_f < \min\{T_c^m, T_c^n\}$, is modeled by solving Eq. (15) for $\bar{A}, \bar{\alpha} < 0$. The initial conditions are randomly chosen values of Q_{11} , Q_{12} , M_1 , and M_2 from the interval $[-0.05, 0.05]$, i.e., a perturbation around the $|\mathbf{Q}| \simeq 0$ and $|\mathbf{M}| \simeq 0$ solution and mimics the disordered phase. The boundary conditions are as before with $\ell'_1 = \ell'_2 = 0.1$, $\xi = 1$, and $c' = 1$, i.e., values of the coupling

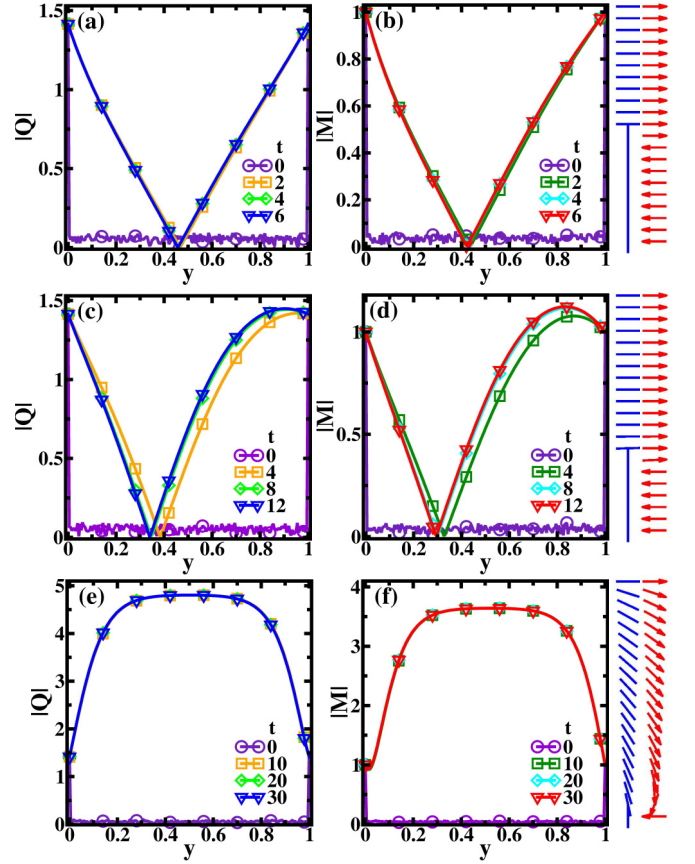


FIG. 5. Evolution of $|\mathbf{Q}|$ and $|\mathbf{M}|$ after a rapid quench with parameters $\mu = 1$, $\ell'_1 = \ell'_2 = 0.1$, $\xi' = 1$, and $c' = 1$ for $\bar{A} = \bar{\alpha} = -0.1$ in (a), (b), $\bar{A} = \bar{\alpha} = -1$ in (c), (d), and $\bar{A} = \bar{\alpha} = -10$ in (e), (f). The data correspond to solutions of Eqs. (15) for different times t . Markers are used to distinguish curves.

parameter that favor polydomain structures as suggested in Fig. 2. We plot the solutions in Fig. 5 for $\bar{A} = \bar{\alpha} = -0.1, -1$, and -10 , interpreted as shallow, moderate, and deep quenches, respectively. We plot the solutions at different times and focus on the long-time behavior; as expected, there are no isotropic polydomains with $\mathbf{Q} = 0$ in these examples since we expect the isotropic regions to become rapidly ordered after quenching to low temperatures and hence isotropic polydomains are not visible for long times. In the case of shallow and moderate quenches, we observe polydomain structures in Figs. 5(a)–5(d). For deeper quenches, the polydomain structure is lost and this can be qualitatively understood as domain walls with $|\mathbf{Q}| = 0$ or $|\mathbf{M}| = 0$ are energetically expensive for low temperatures. The solutions are independent of the initial conditions for the system.

IV. CONCLUSION

We study spatial pattern formation in a one-dimensional confined nematic system with suspended magnetic nanoparticles, using the phenomenological approach in [5,8]. We work in the absence of external magnetic fields and study the effects of confinement, conflicting boundary conditions, elasticities, and magnetonematic coupling. We demonstrate that nematic elasticities, magnetic stiffness, and magnetonematic coupling

can stabilize polydomain structures with opposing states of magnetization without external magnetic fields and generate tailored morphologies, for which \mathbf{M} is aligned with \mathbf{n} and vice versa. We illustrate these effects by means of four parameters: ℓ_1, ℓ_2 interpreted as measures of nematic elasticity and magnetic stiffness, ξ as a measure of magnetic order, and c interpreted as a measure of magnetonematic coupling. Using asymptotic reasoning, we identify two limits: the Ginzburg-Landau limit of small elasticity that excludes polydomain formation and the Laplace limit of strong elasticity and weak magnetonematic coupling that renders polydomain formation in both \mathbf{n} and \mathbf{M} ; these heuristic predictions are validated by numerical results and, in fact, show that Ginzburg-Landau-like effects survive even with moderate values of ℓ_1, ℓ_2 and Laplace-like effects (polydomains) survive provided the magnetonematic coupling constant is not too large, e.g., of the same order of magnitude as ℓ_1, ℓ_2 . In fact, this is our main observation—a set of numerically observed conditions on the four parameters $\{\ell_1, \ell_2, \xi, c\}$ that allow for polydomain formation (Laplace limit) and that disallow polydomain formation, leading to tailored morphologies (Ginzburg-Landau limit) without any external magnetic fields. In doing so, we also provide a simple numerical quenching experiment that demonstrates polydomain formation in \mathbf{M} , i.e., regions of distinct averaged magnetization separated by a domain wall, from largely disordered initial conditions, without any external magnetic fields. The polydomains disappear with increased magnetonematic coupling. There are qualitative analogies between the effects of the magnetonematic coupling and the effects of an external magnetic field aligned along the nematic director \mathbf{n} and, in our simulations, the coupling constant appears to have the same effect as the strength of an external magnetic field [9]. For example, the magnetic domain wall displacement reported in [9] under an applied magnetic field is also observed in our simulations resulting

due to variation in the coupling constant [in Figs. 2(a)–2(d)]. We speculate that our simple framework and numerical results can give informative insight into how to tailor experiments to stabilize and destabilize polydomains according to the experimental needs.

A natural extension of this problem is to study pattern formation induced by boundary conditions and magnetonematic coupling on 2D domains such as squares. This is particularly interesting since it is known that the 2D LdG model admits multiple stable equilibria on a square (see [26]) and a reasonable conjecture is that every equilibrium solution has a counterpart in the coupled (\mathbf{Q}, \mathbf{M}) system, yielding a plethora of possibilities. It is worth pointing out that previous studies have not exploited the effects of geometric frustration or pattern formation driven by inhomogeneous boundary conditions; they have strongly relied on external magnetic fields [8,9,27]. Our work is an interesting example of a coupled MNP-NLC system without external fields and the effects of confinement and magnetonematic coupling on stable configurations can be further enhanced or suppressed by suitably applied external magnetic fields, if necessary. This will be investigated in future work.

ACKNOWLEDGMENTS

K.B. acknowledges CSIR, India for financial support under Grant No. 09/086(1208)/2015-EMR-I. A.M. also acknowledges support from an OCIAM Visiting Fellowship and the Keble Advanced Studies Centre. The authors would like to thank the International Centre for Mathematical Sciences, where they met for the first time, for follow-on funding and would like to thank DST-UKIERI for generous funding to support this three-year collaborative project. The authors gratefully acknowledge the HPC facility of IIT Delhi for the computational resources.

-
- [1] P. G. de Gennes and J. Prost, *The Physics of Liquid Crystals*, International Series of Monographs on Physics (Clarendon Press, Oxford University Press, New York, 1995).
 - [2] V. Fréedericksz and A. Repiewa, *Z. Phys.* **42**, 532 (1927).
 - [3] F. Brochard and P. G. de Gennes, *J. Phys. (France)* **31**, 691 (1970).
 - [4] J. Rault, P. E. Cladis, and J. P. Burger, *Phys. Lett. A* **32**, 199 (1970).
 - [5] A. Mertelj, D. Lisjak, M. Drogenik, and M. Čopič, *Nature (London)* **504**, 237 (2013).
 - [6] Y. L. Raikher, S. V. Burylov, and A. N. Zakhlevnykh, *Zh. Eksp. Teor. Fiz.* **91**, 542 (1986) [*J. Exp. Theor. Phys.* **64**, 319 (1986)].
 - [7] N. Podoliak, O. Buchnev, O. Buluy, G. D'Alessandro, M. Kaczmarek, Y. Reznikov, and T. J. Sluckin, *Soft Matter* **7**, 4742 (2011).
 - [8] G. Zarubin, M. Bier, and S. Dietrich, *Soft Matter* **14**, 9806 (2018).
 - [9] M. Shuai, A. Klittnick, Y. Shen, G. P. Smith, M. R. Tuchband, C. Zhu, R. G. Petschek, A. Mertelj, D. Lisjak, M. Čopič, J. E. Maclennan, M. A. Glaser, and N. A. Clark, *Nat. Commun.* **7**, 10394 (2016).
 - [10] P. Hohenberg and A. Krekhov, *Phys. Rep.* **572**, 1 (2015), an introduction to the Ginzburg-Landau theory of phase transitions and nonequilibrium patterns.
 - [11] S. V. Burylov and Y. L. Raikher, *Mol. Cryst. Liq. Cryst. Sci. Technol., Sect. A* **258**, 107 (1995).
 - [12] G. Zarubin, M. Bier, and S. Dietrich, *J. Chem. Phys.* **149**, 054505 (2018).
 - [13] C. Luo, A. Majumdar, and R. Erban, *Phys. Rev. E* **85**, 061702 (2012).
 - [14] S. Puri and V. Wadhawan, *Kinetics of Phase Transitions* (CRC Press, Boca Raton, FL, 2009), pp. 8–68.
 - [15] S. Ma, *Modern Theory of Critical Phenomena* (Taylor & Francis, London, 2018).
 - [16] H. Pleiner, E. Jarkova, H.-W. Müller, and H. R. Brand, *Magneto hydrodyn.* **37**, 254 (2001).
 - [17] D. Henao, A. Majumdar, and A. Pisante, *Calc. Var. Part. Diff. Eq.* **56**, 55 (2017).
 - [18] *COMSOL Multiphysics® V. 5.3a* (COMSOL AB, Stockholm, Sweden, 2017).
 - [19] A. Majumdar, *Eur. J. Appl. Math.* **21**, 181 (2010).

- [20] G. Canevari, A. Majumdar, and A. Spicer, *SIAM J. Appl. Math.* **77**, 267 (2017).
- [21] M. A. Peletier, [arXiv:1402.1990](https://arxiv.org/abs/1402.1990).
- [22] P. Heller, *Rep. Prog. Phys.* **30**, 731 (1967).
- [23] F. Keffer, in *Ferromagnetism/Ferromagnetismus*, edited by H. P. J. Wijn (Springer, Berlin, Heidelberg, 1966), pp. 1–273.
- [24] S. Singh, *Phys. Rep.* **324**, 107 (2000).
- [25] P. J. Collings and M. Hird, *Introduction to Liquid Crystals: Chemistry and Physics*, Liquid Crystals Book Series (CRC Press, Boca Raton, FL, 1997).
- [26] M. Robinson, C. Luo, P. E. Farrell, R. Erban, and A. Majumdar, *Liq. Cryst.* **44**, 2267 (2017).
- [27] A. Mertelj, N. Osterman, D. Lisjak, and M. Čopič, *Soft Matter* **10**, 9065 (2014).